1 # Wet-environment Evapotranspiration and Precipitation Standardized Index
2 # (WEPSI) for drought assessment and monitoring

3 **A. Khoshnazar[1], G. A. Corzo Perez[1], V. Diaz[1,2], and M. Aminzadeh[3]**

4 [1]IHE Delft Institute for Water Education, The Netherlands

5 ali.khoshnazaar@gmail.com; a.khoshnazar@un-ihe.org (AK)

6 g.corzo@un-ihe.org (GACP)

7 [2]Water Resources Section, Delft University of Technology, The Netherlands;
8 v.diazmercado@tudelft.nl; vitalidime@gmail.com (VD)

9 [3]Department of Civil Engineering, Isfahan University of Technology, Iran;

10 m.aminzadeh@iut.ac.ir (MA)

11 Corresponding author: Vitali Diaz (v.diazmercado@tudelft.nl; vitalidime@gmail.com), Ali
12 Khoshnazar (ali.khoshnazaar@gmail.com; a.khoshnazar@un-ihe.org)

13

14 **Key Points:**

15 - We introduce the Wet-environment Evapotranspiration and Precipitation Standardized
16   Index (WEPSI)

17 - WEPSI highly correlates with the well-known hydrological drought index SRI

18 - Droughts calculated with WEPSI coincide with the declines in crop cereal production in
19   the region

20

21 **Keywords:** WEPSI; drought index; drought assessment; drought monitoring; drought analysis;
22 agricultural drought; wet-environment evapotranspiration; WEAP; Lempa River basin; mutual
23 information; ONI
24

25   **Abstract**

26   Drought is a major threat to global agriculture and can trigger or intensify food price increase and
27   migration. Assessment and monitoring are essential for proper drought management. Drought
28   indices play a fundamental task in this respect. This research introduces the Wet-environment
29   Evapotranspiration and Precipitation Standardized Index (WEPSI) for drought assessment and
30   monitoring. WEPSI is inspired by the Standardized Precipitation Evapotranspiration Index (SPEI),
31   in which water supply and demand are incorporated into the drought index calculation. WEPSI
32   considers precipitation (P) for water supply and wet-environment evapotranspiration (ET_w) for
33   water demand. We use an asymmetric complementary relationship to calculate ET_w using actual
34   (ET_a) and potential evapotranspiration (ET_p). WEPSI is tested in the transboundary Lempa River
35   basin located in the Central American dry corridor. ET_w is estimated based on evapotranspiration
36   data calculated using the Water Evaluation And Planning (WEAP) system hydrological model. To
37   investigate the performance of our introduced drought index, we compare it with two well-known
38   meteorological indices (Standardized Precipitation Index and SPEI), together with a hydrological
39   index (Standardized Runoff Index), in terms of correlation and mutual information (MI). We also
40   compare drought calculated with WEPSI and historical information, including crop cereal
41   production and Oceanic Niño Index (ONI) data. The results show that WEPSI has the highest
42   correlation and MI compared with the three other indices used. It is also consistent with the records
43   of crop cereal production and ONI. These findings show that WEPSI can be applied for agricultural
44   drought assessments.

45   **1 Introduction**

46   Drought affects around 40% of the global land area and is a major threat to global
47   agriculture (Wang et al., 2011; Wen et al., 2021). It can trigger or intensify wildfire, water scarcity,
48   crop damage, food price increase, migration, and adverse health impacts (Mukherjee et al., 2018).
49   Drought monitoring is crucial to pre-pare for drought and mitigate its negative effects. In this
50   regard, drought indices are useful measures for scientists and decision makers to monitor, assess,
51   and manage drought.

52   Although there exists no unique standard definition for drought (Wang et al., 2020;
53   Yihdego et al., 2019), it is described as the deficit in precipitation (P) compared with an average
54   within a period (Yihdego et al., 2019). The combination of anomalies in P and temperature, known
55   as meteorological drought, leads to soil moisture deficit, referred to as agricultural drought, and a
56   lack of water in lakes and streams, defined as hydrological drought (Mukherjee et al., 2018; Wilhite
57   and Glantz, 1985). Agricultural and hydrological droughts are usually the subsequent phases of
58   meteorological drought (Yihdego et al., 2019).

59   A drought index aims to quantify drought severity and help in the identification and
60   characterization of drought development by assimilating a hydrometeorological dataset into
61   numerical values that indicate the magnitude of water anomalies (Yihdego et al., 2019). Selecting
62   a proper drought index for drought assessment and monitoring is not always trivial and involves
63   different challenges. The following considerations should be made when selecting the drought
64   index. (1) The drought index must follow the standardization of the hydrometeorological variable
65   used. Otherwise, in contiguous regions, the same drought index can show different drought
66   conditions, making it difficult to calculate drought onset and spatial extent (Yihdego et al., 2019).
67   (2) It is preferable that the methodology for the calculation is clear and that the fewest possible
68   inputs are used. Some drought indices are not usable every-where. Some others require many

69 inputs or have complex structures that make their implementation difficult (Yihdego et al., 2019).
70 (3) It is desirable if the drought index can identify different types of droughts. Some drought
71 indices can detect various types of droughts, making them have a broader range of applications
72 (Yihdego et al., 2019).

73   Much academic effort has been devoted to introducing appropriate drought indices. As an
74 early attempt, Palmer (Palmer, 1965) proposed a regional index to determine meteorological and
75 agricultural droughts, known as the Palmer Drought Severity Index (PDSI). The PDSI uses
76 temperature, soil moisture, and P. The structure of the PDSI does not allow for comparison across
77 different regions. Time scale limitation and data complexity are also high-lighted deficiencies of
78 the PDSI (Yihdego et al., 2019). Based on these drawbacks, three years later, Palmer introduced
79 his Crop Moisture Index (CMI) for agricultural drought (Palmer, 1968). The self-calibrated Palmer
80 Drought Severity Index (scPDSI), proposed by Wells et al. (Wells et al., 2004), is another index
81 based on the PDSI but allows comparison of different regions.

82   One of the most outstanding advances in developing drought indices was made by McKee
83 et al. (McKee et al., 1993). They proposed one of the most well-known drought indices, the
84 Standardized Precipitation Index (SPI). The SPI is popular because of its simple structure. It can
85 be calculated with the presence of missing data. The SPI has the flexibility of calculation in short
86 or long time steps (aggregation periods), which is especially advantageous in monitoring different
87 types of droughts (Vicente-Serrano et al., 2010; Yihdego et al., 2019). Nevertheless, the SPI
88 overlooks the role of other important variables, such as evapotranspiration (ET) (Mukherjee et al.,
89 2018; Vicente-Serrano et al., 2010), and it cannot reflect the in-crease in water demand because of
90 temperature. In response to this limitation, Vicente-Serrano et al. (2010) introduced another widely
91 used drought index, the Standardized Precipitation Evapotranspiration Index (SPEI). The SPEI
92 uses the SPI's structure but applies temperature and P. This drought index can capture agricultural
93 drought more efficiently than SPI can, as it uses potential evapotranspiration (ET_p) (Yihdego et
94 al., 2019). However, the SPEI may face limitations when comparing drought across different
95 climate regions (Mukherjee et al., 2018).

96   P is the basis for the calculation of many drought indices. At different time aggregations,
97 P can help indicate all types of droughts. It is relatively the most direct variable of water supply
98 (Yihdego et al., 2019). However, using only P leads to a failure to incorporate the changes in
99 available energy, air humidity, and wind speed; consequently, it can provide values that do not
100 capture reality (Mukherjee et al., 2018). Drought relies not only on water supply but also on water
101 demand, for which ET can be the proxy (Speich, 2019). ET forces around 60% of the land P to
102 return to the atmosphere (Zhang et al., 2020) and creates two-thirds of the planet's annual P. It
103 also consumes more than half of the solar energy absorbed by the land surface as latent heat.
104 Accordingly, ET, which contributes to mass and energy exchange between land and atmosphere
105 (Zhang et al., 2020), is crucial in improving our vision of land–atmosphere interactions and the
106 terrestrial water cycle (Xiao et al., 2020; Zheng et al., 2019). These explain ET's important role in
107 releasing droughts (Mukherjee et al., 2018) and drought severity at both the local and global scales
108 (Dhungel and Barber, 2018; Zhang et al., 2020). Therefore, using ET together with P in the
109 structure of drought indices allows a more comprehensive drought assessment (Lu et al., 2019;
110 Zargar et al., 2011).

111   ET has several types, and selecting its type is highly critical in defining the drought index.
112 For instance, the so-called Standardized Precipitation Actual Evapotranspiration Index uses actual
113 evapotranspiration (ET_a) in its structure (Homdee et al., 2016). However, the difference be-tween

114 P and ET_a could not capture the real water shortage (WS). This is because ET_a is not the ultimate
115 possible amount of ET but the real ET occurring on the surface (Kim and Rhee, 2016; Vicente-
116 Serrano et al., 2018). As one of the other types of ET, ET_p, which has already been used in the
117 structure of some drought indices in the literature, is a measure of atmospheric evaporative demand
118 (Dash et al., 2021; Kim and Rhee, 2016; Vicente-Serrano et al., 2018; Yihdego et al., 2019). Wet-
119 environment evapotranspiration (ET_w) is ET from an extensive, well-watered surface into the
120 atmosphere (Aminzadeh et al., 2016; Kahler and Brutsaert, 2006).

121 To specify the appropriate water demand term for drought assessment, it is essential to be
122 aware of both water balance and energy balance (Koppa et al., 2021). The literature in this area is
123 rich, and among existing studies is the rigorous work conducted by Fisher et al. (Fisher et al.,
124 2011), which has taken a proper look into the concept.

125 Based on water balance in a closed system (e.g., a watershed), where P is the only water
126 supply, the supplied water takes one of the following forms (human systems, extraction by insects
127 or animals, and leaking into the earth's deep crust are not part of this scope):

128 1) Going into the soil and Ground-Water flow or recharge (GW); 2) surface Runoff (R); 3)
129 being Stored in lakes, ponds, and plants (S); and 4) going back to the atmosphere (ET_a). The water
130 balance equation is expressed as follows:

131 $$P = GW + R + S + ET_a \qquad (1)$$

132 The upper limit of ET_a in water balance is ET_w and will occur only if enough water is
133 supplied (Fisher et al., 2011). ET_w changes by energy variation. Then, we can define water loss
134 via ET as follows:

135 $$P - ET_a = GW + R + S \qquad (2)$$

136 Apparently, we always have $P - ET_a \geq P - ET_w$.

137 Then, one can claim that ET_w illustrates the real ET demand.

138 Despite its important role as an indicator of water demand, the use of ET_w in the structure
139 of P-based drought indices has been almost overlooked in the literature. Incorporating ET_w in
140 drought index calculations, especially for agricultural purposes, is advantageous. It captures a more
141 realistic condition in which the important role of ET as water demand is neither underestimated
142 nor overestimated by using a pessimistic indicator.

143 As a robust and generalized drought index running through a simple structure is essential
144 for improving water resource management and planning (Yihdego et al., 2019), this research
145 introduces the Wet-environment Evapotranspiration and Precipitation Standardized Index
146 (WEPSI). WEPSI is inspired by the SPEI, in which water supply and demand are incorporated
147 into the drought index calculation. WEPSI follows the SPI methodology for its calculation, while
148 P is considered for water supply and ET_w for water demand. Priestley and Taylor's model (P-T
149 model) (Priestley and Taylor, 1972) is widely used as a proxy of ET_w (Kahler and Brutsaert, 2006).
150 This model has a coefficient that was proposed to account for the drying power of the air, with an
151 estimated mean value of 1.26 (or $\alpha = 1.26$) over saturated surfaces, such as oceans. Recent research
152 has shown that this coefficient is impacted by the radiation regime, relative humidity, air
153 temperature, wind speed, and geographical site. This raises doubts about the use of P-T model
154 outputs without calibration of its coefficient (Aminzadeh and Or, 2014). Accordingly, we used an
155 asymmetric Complementary Relationship (CR) to obtain ET_w using ET_a and ET_p, based on our

156 reliable data (Khoshnazar et al., 2021). To evaluate the performance of WEPSI, we first compared
157 its results with both well-known drought indices (SPI, SPEI), as well as with the Standardized
158 Runoff Index (SRI). The coefficient of determination and mutual information (MI) were used for
159 this comparison. Additionally, the fluctuation in cereal and crop production in El Salvador, as well
160 as El Niño Southern Oscillation (ENSO) events, was compared to drought calculated using
161 WEPSI, illustrating its performance, especially for agricultural purposes. We assessed WEPSI at
162 the catchment scale using ET data calculated from the Water Evaluation And Planning (WEAP)
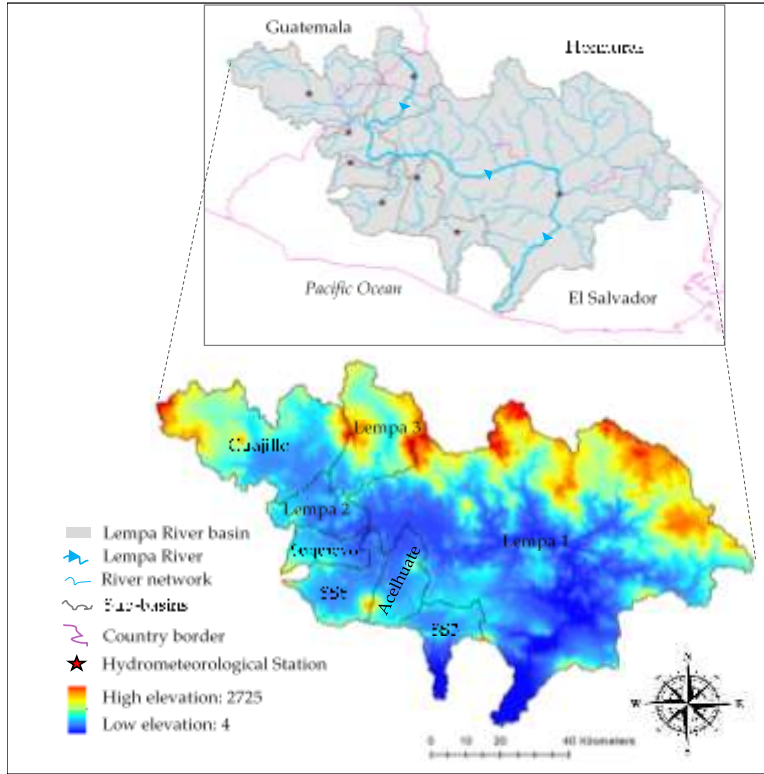163 system hydrological model.

164 The remainder of the paper is organized as follows. In Section 2, Materials and Methods,
165 we start with our case study area. Then, the WEAP model and benchmark drought indices are
166 provided. As the core of this section, WEPSI is introduced, and the experimental setup is presented.
167 The results and discussion are given in Section 3. Finally, Section 4 concludes the paper and
168 suggests directions for future research.

169 **2 Materials and Methods**

170 2.1 Case study

171 The transboundary Lempa River basin located in the Central American dry corridor is used
172 as our case study area in investigating WEPSI. With a length of 422 km, the Lempa River is the
173 longest stream in Central America. It originates from volcanic mountains in Guatemala, with 1,500
174 masl elevation, and flows to the Pacific Ocean in El Salvador. Around 360.2 km (85%) of the
175 river's length flows into El Salvador's territory (Hernández, 2005). This river flows through
176 Guatemala, Honduras, and El Salvador (Figure 1). The area of the tri-national basin is 17,790 km^2,
177 of which 10,082 km^2 belongs to El Salvador (49% of El Salvadorian land). The basin has a daily
178 average temperature of 23.5°C, a total annual rainfall average of 1,698 mm, and a yearly R of
179 19.21 dm^3 s^{-1} km^2.

180 The Lempa River streamflow has dropped by 70% (Helman and Tomlinson, 2018;
181 Jennewein and Jones, 2016) during the dry years. This is while El Salvador gains 68% of its surface
182 water from this river basin (El Salvador's Ministry of Environment and Natural Resources
183 (MARN), 2019). The basin environs 13 of 14 departments of El Salvador, including 3,967,159
184 inhabitants (77.5% of the country's population). Alterations in the hydrological regime, such as
185 extreme events (e.g., drought and tropical cyclone), worsen water quality and quantity in the region
186 ("Fostering Water Security in the Trifinio Region: Promoting the formulation of a TDA/SAP for
187 its transboundary Lempa River Basin.," 2019). The current condition of the basin highlights the
188 need for water resource management and drought assessment.

189

190 **Figure 1.** Lempa River basin location (Khoshnazar et al., 2021).

191 2.2 WEAP model

192 The WEAP system is a well-known model for water resource planning developed by the
193 Stockholm Environment Institute (Seiber and Purkey, 2015). WEAP allows the calculation of
194 terrestrial hydrological cycle variables, such as R, infiltration, and ET. We used WEAP-derived
195 ET to calculate WEPSI. The required input data on hydrometeorological and soil characteristics
196 of the model were obtained from MARN for the period 1980–2010 (MARN, 2020). Based on basin
197 management by local authorities and physiographic characteristics, the Lempa River basin was
198 divided into the following eight sub-basins: Lempa 1, Lempa 2, Lempa 3, Guajillo, Suquioyo,
199 Acelhuate, SS6, and SS3 (Figure 1). Khoshnazar et al. (Khoshnazar et al., 2021) showed that the
200 WEAP-derived variables are reliable for drought assessment in the Lempa River basin. For the
201 description of the validation and calibration procedure of the model, interested readers are referred
202 to our previous publication (Khoshnazar et al., 2021).

203 Five methods to simulate basin processes, such as ET, R, and irrigation demands, are
204 available in WEAP. In our research, we use the soil moisture method, which considers that the
205 basin has two soil layers (buckets or tanks). The top soil layer is considered shallow-water
206 capacity, and the bottom soil layer is considered deep-water capacity. Figure 2 depicts a conceptual
207 diagram of the soil moisture method (Seiber and Purkey, 2015). The water balance is calculated
208 for each fraction area *j* for the first layer, assuming that the climate is steady in each sub-basin.
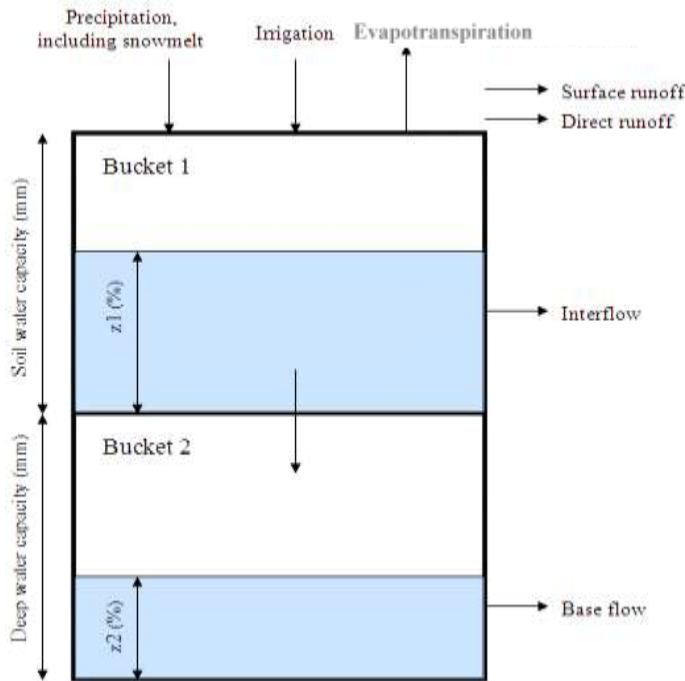209 The water balance is calculated using Eq. (3) as follows (Oti et al., 2020):

210 $$Rd_j \frac{dZ_{1,j}}{dt} = P_e(t) - ET_p(t)k_{c,j}(t)\left(\frac{5Z_{1,j}-2Z_{1,j}^2}{3}\right) - P_e(t)Z_{1,j}^{RRF_j} - f_j k_{s,j}Z_{1,j}^2 - (1-f_j)k_{s,j}Z_{1,j}^2 \qquad (3)$$

211   where $Z_{1,j}$ is the relative storage based on the total effective storage of the root zone. Rd_j is
212   the soil holding capacity of the land cover fraction j (mm). ET_p is calculated using the modified
213   Penman–Monteith reference crop ET_p with the crop/plant coefficient ($k_{c,j}$). P_e is the effective
214   precipitation (P), and RRF_j is the R resistance factor of the land cover. $P_e(t)Z_{1,j}^{RRF_j}$ is indicated as
215   the surface R. $f_j k_{s,j} Z_{1,j}^2$ shows the interflow from the first layer, for which the term $k_{s,j}$ denotes the
216   root zone saturated conductivity (mm/time), and f_j is the partitioning coefficient that considers
217   water horizontally and vertically based on the soil, land cover, and topography. Finally, the term
218    $(1 - f_j)k_{s,j}Z_{1,j}^2$ is percolation. WEAP uses Eq. (4) to calculate ET_a (Kumar et al., 2018):

219        $$ET_a = ET_p \frac{(5z_1 - 2z_2^2)}{3} \tag{4}$$

220   where z_1 and z_2 are the water depth of the top and bottom soil layers (bucket), respectively
221   (Figure 2).

222   We calculated the monthly ET_w with the WEAP-derived ET_p and ET_a following the
223   procedure presented in Section 2.4.2 for each sub-basin.

224

225   **Figure 2.** Conceptual diagram of the water balance calculation in WEAP (Seiber and
226   Purkey, 2015).

227   2.3 Drought indices for comparison

228   We compare SPI and SPEI meteorological drought indices with WEPSI. As discussed, SPI
229   is based on the total amount of water (i.e., P), whereas SPEI incorporates the reduction of water
230   based on ET_p. Then we compare these three indices (SPI, SPEI, and WEPSI) with SRI, which is a
231   hydrological drought index and reflects the real water availability on land. The application of a
232   hydrological drought index can provide us with further insights into the situation of the studied
233   area compared with using only meteorological drought indices (Shukla and Wood, 2008). On the

234   other hand, based on the water balance equation, SRI implicitly reflects ET_a (Vicente-Serrano et
235   al., 2010). Accordingly, when a meteorological drought index reflects a high similarity with SRI,
236   it provides more insights into the hydrological situation of the land and is closer to the real
237   evapotranspiration condition. Such an index has a higher potential to be used solely without
238   requiring a complementary hydrological index and, consequently, eliminates the difficulty of
239   gathering and modeling hydrological data.

240   The methodology for calculating these drought indices is as follows.

2.3.1 The Standardized Precipitation Index (SPI)

242   The methodology for calculating the SPI is presented as follows (McKee et al., 1993).
243   Based on long-term P data (30 years or more), a time scale (also known as aggregation period) is
244   specified. This time scale can be 3, 6, 9, 12, 24, or 48 months. Then, the aggregated P is fitted to
245   a distribution function. Afterward, the cumulative probability function is equal to that of the
246   normal distribution, for which the standardized variable with zero mean and unity standard
247   deviation is obtained. The literature suggests the Gamma distribution as one of the best choices for
248   SPI calculation (Kim et al., 2019; McKee et al., 1993). Therefore, we have used Gamma
249   distribution for SPI calculation, as well.

2.3.2 The Standardized Precipitation Evapotranspiration Index (SPEI)

251   The SPEI follows the SPI methodology but uses the difference between P and ET_p as its
252   input (Vicente-Serrano et al., 2010). Several studies have shown that the log-logistic distribution
253   is appropriate for SPEI calculation (Vicente-Serrano et al., 2010). Accordingly, we have used the
254   three-parameter log-logistic (LL3) distribution for obtaining the SPEI.

2.3.3 The Standardized Runoff Index (SRI)

256   The SRI uses R as input and follows a similar procedure as SPI (Shukla and Wood, 2008).
257   McKee et al. (McKee et al., 1993) proposed a gamma distribution for the SPI and suggested that
258   this distribution is operational for other variables related to drought (Sorí et al., 2020).
259   Accordingly, we have used the Gamma distribution to calculate SRI, utilizing R data obtained
260   from the WEAP model.

2.4 The Wet-environment Evapotranspiration and Precipitation Standardized Index (WEPSI)

2.4.1 WEPSI calculation

264   WEPSI is calculated following the SPI methodology to standardize the input, except that
265   WEPSI uses WS instead of P alone.

266   WS is calculated as the difference between P (water supply) and ET_w (water demand) (Eq.
267   (5)).

268         $$WS = P - ET_w \qquad\qquad\qquad (5)$$

269   WEPSI is inspired by the structure of the SPEI that uses ET_p to incorporate water demand
270   into the drought index calculation. Based on our discussions in the previous section, ET_w can be
271   an appropriate representative of water demand. Accordingly, we incorporate ET_w into WEPSI as
272   the water demand indicator and P to account for the water supply. Since WEPSI incorporates $P -$

273   ET_w as its input and concerning the water balance equation (Eq. (1)), we anticipate that our
274   proposed drought index should have a higher correlation with SRI and, therefore, can provide
275   useful information about the hydrological situation of the area. We will later investigate this in the
276   numerical results.

277   As LL3 distribution has shown good performance in SPEI calculation and similar drought
278   indices, we consider LL3 distribution to fit WS in WEPSI calculation (Kim and Rhee, 2016;
279   Vicente-Serrano et al., 2010). Similar to SPI, WEPSI can be obtained based on different time steps,
280   such as 3, 6, 9, 12, 24, and 48 months.

281   Since WEPSI follows the structure of the SPI, we consider the same drought categorical
282   classification (Table 1).

283   **Table 1.** Drought categorical classification using WEPSI

WEPSI value	Drought/Wet category
≥ 2	Extreme wet
1.5 to 2	Severe wet
1 to 1.5	Moderate wet
0 to 1	Low wet
−1 to 0	Low drought
−1.5 to −1	Moderate drought
−2 to −1.5	Severe drought
≤ -2	Extreme drought

284   ET_w used in Eq. (5) is calculated based on the methodology introduced in the following
285   subsection.

286   2.4.2 ET_w calculation

287   As previously mentioned, we have used CR to obtain ET_w data. Based on the Bouchet
288   hypothesis (Bouchet, 1963), equilibrium evapotranspiration or ET_w is equal to ET_a and ET_p under
289   saturated conditions. A saturated condition refers to an extensive, well-watered surface where
290   input energy is the limiting factor (Xiao et al., 2020). We always have $ET_a \leq ET_w$ and $ET_p \geq ET_w$.
291   ET_w, ET_p, and ET_a have been related to one another by what is known as CR. A general form for
292   CR is suggested by Kahler and Brutsaert (Kahler and Brutsaert, 2006) (Eq. (6)).

293           $$(1 + b)ET_w = bET_a + ET_p \qquad (6)$$

294   where b is an empirical constant, and ET_a, ET_p, and ET_w are the actual, potential, and wet-
295   environment evapotranspiration, respectively.

296   The symmetric CR considered by Bouchet is obtained by taking $b = 1$ in Eq. (6). However,
297   the literature indicates that b generally exceeds and is rarely equal to 1 (i.e., CR is asymmetric)
298   (Aminzadeh et al., 2016). Consequently, for the ET_w calculation, in addition to ET_p and ET_a, it is
299   necessary to estimate the value of b.

300   Eq. (6) can be rewritten in terms of b (Aminzadeh et al., 2016).

301           $$b = \frac{ET_p - ET_w}{ET_w - ET_a} \qquad (7)$$

302   Eq. (7) shows that the increase in ET_p above ET_w is proportional to the energy flux provided
303   by surface drying and the decrease in evaporation rate.

304   Normalizing Eq. (7) results in Eq. (8) and Eq. (9) (Aminzadeh et al., 2016),

305     $$ET_{a+} = \frac{(1+b)ET_{MI}}{1+bET_{MI}} \qquad (8)$$

306     $$ET_{p+} = \frac{1+b}{1+bET_{MI}} \qquad (9)$$

307   where $ET_{a+} = \frac{ET_a}{ET_w}$, $ET_{p+} = \frac{ET_p}{ET_w}$, $ET_{MI} = \frac{ET_a}{ET_p}$, and ET_{MI} is the surface moisture index
308   (with a maximum of 1). ET_{a+} and ET_{p+} are the scaled actual and ET_p, respectively. Figure 3
309   illustrates the variation in the scaled actual and potential evapotranspiration with respect to
310   different values of the surface moisture index.

311   The b parameter in Eq. (8) and (9) can be obtained from Eq. (10) (Aminzadeh et al., 2016;
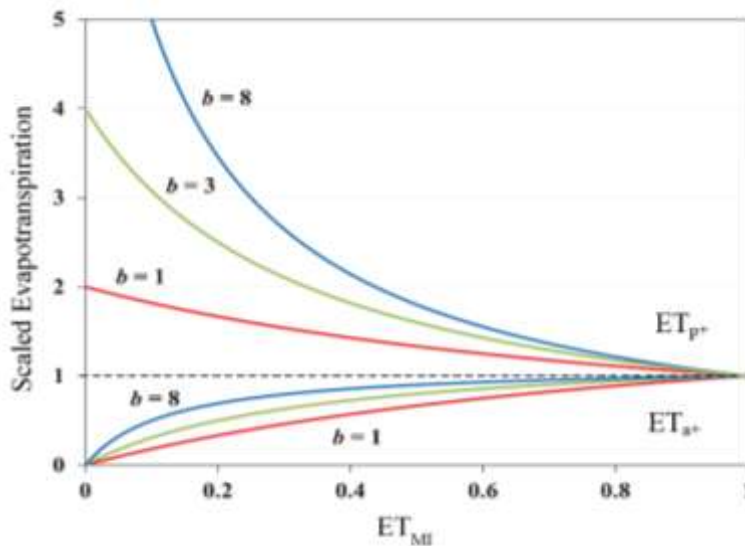312   Granger, 1989; Xiao et al., 2020),

313     $$b = \frac{1}{\gamma} \frac{e_s^* - e_w^*}{T_s - T_w} \qquad (10)$$

314   where e_s^* is the saturated vapor pressure at surface temperature Ts, and e_w^* is the saturated
315   vapor pressure at a hypothetical wet surface temperature Tw. The psychometric constant γ (in
316   k Pa °C^{-1}) is calculated with the atmospheric pressure (Pe) as $\gamma = 0.665 \times 10^{-3}$ Pe, with Pe in
317   kPa.

318   Alternatively, to facilitate the calculation of CR, Aminzadeh et al. (Aminzadeh et al., 2016)
319   suggested an atmospheric input-based equation for b (Eq. (11)), which is more straightforward
320   than Eq. (10) (Han and Tian, 2020); this is why we have used this equation in our paper.

321     $$b = A\,R_{S,net} + B \qquad (11)$$

322   where $R_{S,net}$ is the net shortwave radiation flux in W m^{-2}. $R_{S,net}$ is calculated with the
323   incoming shortwave radiation flux RS and the surface albedo α as $R_{S,net} = (1 - \alpha)R_s$.

324

325   **Figure 3.** Scaled actual (ET_{a+}) and potential evapotranspiration (ET_{p+}) with respect to the
326   surface moisture index (ET_{MI}) variations for different values of *b* (Aminzadeh et al., 2016; Kahler
327   and Brutsaert, 2006).

328   A is a function of wind speed u_a (in m.S^{-1}) (Eq. (12)).

329    $$A = (3u_a + 2) \times 10^{-3} \qquad (12)$$

330   Finally, the B parameter is calculated as a function of wind speed (u_a) and vapor
331   concentration (c_a(kg m^{-3})) (Eq. (13)).

332    $$B = (24.3\, u_a - 1.44)(c_a + 22 \times 10^{-3}) + 0.3 \qquad (13)$$

333   To calculate b using Eq. (11), $R_{S,net}$, u_a, and c_a are required, which can be obtained from
334   meteorological measurements, the literature, or empirical equations.

335   2.5 Experimental setup

336   2.5.1 WEPSI calculation at the catchment scale

337   WEPSI is applied in the Lempa River basin; we have calculated it for each sub-basin
338   (Section 2.1). Eq. (6) is used to obtain ET$_w$.

339   To derive ET$_w$ from Eq. (6), we first applied Eq. (11) to calculate parameter b for 12 months
340   of the year in each sub-basin. In this order, the daily datasets of wind speed (u_a), net shortwave
341   radiation ($R_{S,net}$), and vapor concentration (c_a) for 31 years (1980–2010) and for each sub-basin
342   are used to calculate the monthly average of these three inputs. The meteorological data u_a, $R_{S,net}$,
343   and c_a were retrieved from MARN (MARN, 2020). The ranges of the obtained b values are
344   validated by comparing them with the values available in the literature (Aminzadeh et al., 2016).

345   After obtaining b, we used the time series of WEAP-derived ET$_p$ and ET$_a$ (Section 2.2) as
346   the inputs of Eq. (6) to calculate ET$_w$ in each sub-basin.

347   Finally, with the catchment-wide P and ET$_w$, we computed WEPSI for the time steps 3, 6,
348   9, and 12 months, which are indicated as WEPSI03, WEPSI06, WEPSI09, and WEPSI12,
349   respectively.

350   2.5.2 WEPSI performance evaluation

351   To compare WEPSI in calculating drought, we have used SPI and SPEI, two vastly applied
352   meteorological drought indices. In drought studies, the SPEI has also been applied to agricultural
353   drought assessments. We further utilized the SRI as a hydrological drought index to investigate
354   whether WEPSI could provide insights into the hydrological situation. For the calculation of the
355   SPI, SPEI, and SRI, we followed the methodology presented in Section 2.3. The catchment-wide
356   P, ET$_p$, and R derived from the WEAP model were the inputs used to compute the drought indices
357   for each sub-basin. These three drought indices were similarly calculated for the time steps 3, 6,
358   9, and 12 months. The same notation used in WEPSI is utilized in this case. Therefore, for instance,
359   the 6-month time step for the SPI, SPEI, and SRI is indicated as SPI06, SPEI06, and SRI06,
360   respectively.

361   The comparison is carried out in the following steps. First, a metric commonly used in the
362   performance evaluation of drought indices is applied to compare WEPSI, SPI, SPEI, and SRI,
363   which is the coefficient of determination (r^2) calculated using Eq. (14) as follows:

364    $$r^2 = \left(\frac{\sum_{i=1}^{n}(x_i - \bar{x})(y_i - \bar{y})}{\sqrt{\sum_{i=1}^{n}(x_i - \bar{x})^2 \sum_{i=1}^{n}(y_i - \bar{y})^2}}\right)^2 \qquad (14)$$

365   where x_i and y_i indicate the reference variable and the variable to compare, respectively,
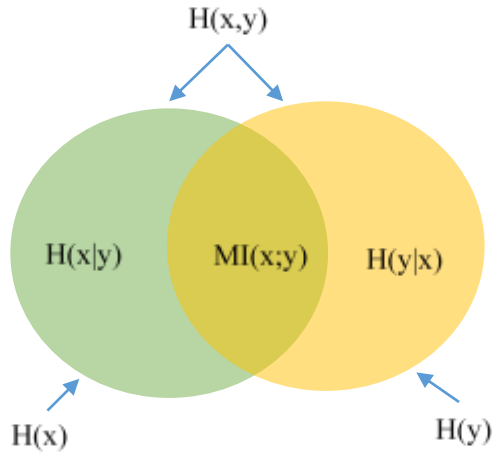366   and $\bar{x}$ and $\bar{y}$ indicate the mean of such values.

367   Second, we use the concept of MI to complement our evaluation, where MI is calculated
368   between WEPSI, SPI, SPEI, and SRI. MI is calculated between two variables to determine the
369   amount of information one variable has about the other (Vergara and Estévez, 2014). This
370   concept is valuable in our comparison procedure, as we seek to know how much information is
371   available about the others in each drought index. MI is calculated using Eq. (15) (Interested
372   readers are referred to Vergara and Estévez (2014) and Al Balasmeh et al. (2020) for the
373   theoretical background underlying the calculation of MI).

374     $$\text{MI}(x; y) = \text{H}(x) - \text{H}(x|y) = \sum_{i=1}^{n} \sum_{j=1}^{n} p\big(x(i), y(j)\big) \cdot \log\left(\frac{p(x(i), y(j))}{p(x(i)) \cdot p(y(j))}\right) \quad (15)$$

375   where $\text{MI}(x; y)$ is the MI between variable x and y, $\text{H}(x)$ is the entropy of a discrete
376   random variable x, $\text{H}(x|y)$ is the conditional entropy of two discrete random variables of x and y,
377     $p(x)$ denotes the probability of the random variable x, and $p(x, y)$ is the joint probability of the
378   random variables of x and y. MI is zero if x and y are statistically independent, and $\text{MI}(x; y) =$
379     $\text{MI}(y; x)$.

380   The unit of information or entropy is nat (natural unit of information), which is based on
381   natural logarithms and powers of e instead of the base two logarithms and powers of two used in
382   the bit unit.

383   Figure 4 shows the Venn diagram based on Eq. (15), which schematizes the relationship
384   between MI and entropies (H) between the random variables x and y.

385

386   **Figure 4.** Venn diagram of the relationship between mutual information (MI) and entropy
387   (H).

388   As drought is an important environmental driver that leads to cereal loss in both yield and
389   quality worldwide (Karim and Rahman, 2015), we also compare the cereal production data of El
390   Salvador with the results of the drought indices in this research.

391   With the time series of WEAP-based WEPSI calculated in each sub-basin, we compute the
392   time series of the percentage of drought area (PDA) for the entire basin. PDAs were calculated
393   monthly as the ratio between the area of sub-basins in drought and the total area of the basin. A
394   drought event starts once the drought index value goes below a threshold and ends as the value
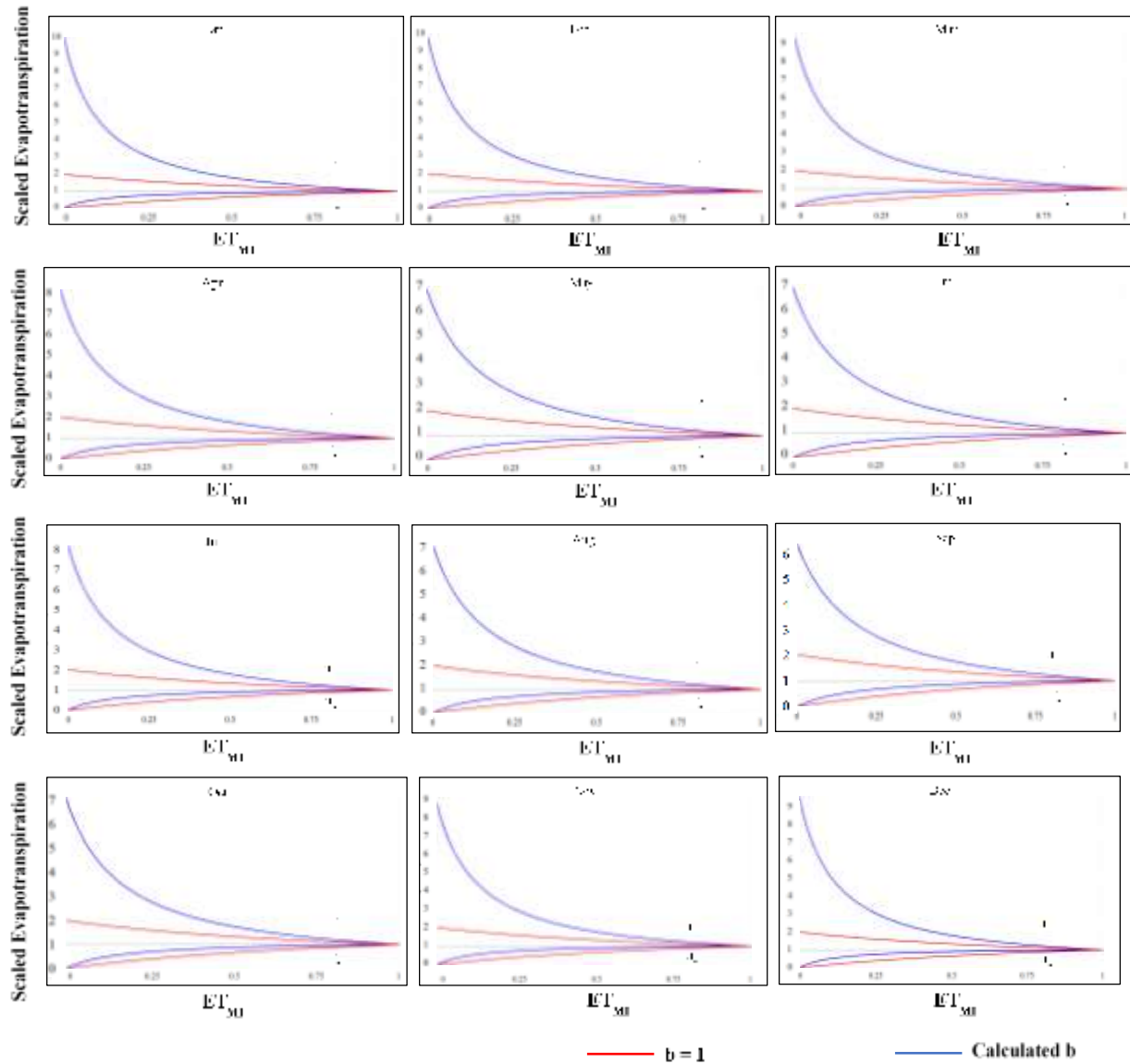
395   rises above the threshold again (Brito et al., 2018; Corzo Perez et al., 2018; Corzo Perez et al.,
396   2011; Diaz et al., 2020). The threshold used in this application was drought index = −1, which is
397   a threshold commonly used in drought assessments (Diaz et al., 2020; Khoshnazar et al., 2021).

398   Finally, we compared PDA fluctuations with El Niño–La Niña years and with El
399   Salvadorian cereal production. Cereal production is used because a lack of soil moisture can lead
400   to a severe reduction in cereal production. On the other hand, drought causes yield and quality loss
401   of cereal globally. Then, if WS, and thereby WEPSI, can capture the status of soil moisture and
402   drought, there should exist a relationship between WEPSI and cereal production (Khoshnazar et
403   al., 2021; Lewis et al., 1998).

404   **3 Results and discussion**
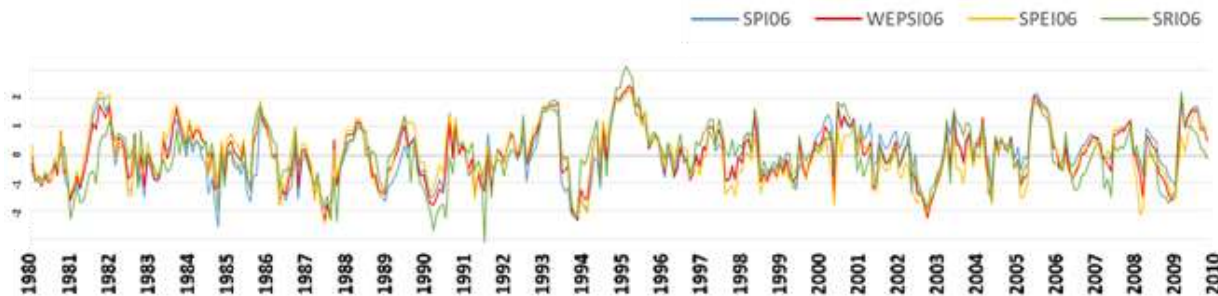
405   3.1. WEPSI calculation and performance evaluation

406   CR was used to calculate the ET_w dataset as follows. The b parameter was calculated
407   following the methodology presented in Section 2.4.2 for 12 months in eight sub-basins. Figure 5
408   depicts the asymmetric CR between ET_{a+} and ET_{p+} as functions of ET_{MI} for 12 months of the year
409   in the Guajillo sub-basin. This figure also shows the symmetric CR that would occur if *b* was equal
410   to 1. As Figure 5 illustrates, compared with the symmetric CR, the calculated b leads to a
411   considerable difference between the scaled evapotranspiration (ET_{a+} and ET_{p+}) as the surface dries
412   and ET_a decreases (Aminzadeh et al., 2016). Figure 5 also highlights the importance of using local
413   and temporal meteorological data (net shortwave radiation, wind speed, and vapor concentration),
414   which can lead to a more accurate approximation of CR and, consequently, of ET_w.

415

416   **Figure 5.** Scaled actual (ET_{a+}) and potential evapotranspiration (ET_{p+}) with respect to the
417 surface moisture index (ET_{MI}) in the Guajillo sub-basin for 12 months of the year.

418

419

420

421

422

423

424

425

426   Figure 6 shows the time series of SPI06, SPEI06, SRI06, and WEPSI06 in the Guajillo
427 sub-basin as an example of the calculation of the drought indices. Our results demonstrate that in
428 61% of the cases, the value of WEPSI06 is larger than that of SPEI06 (i.e., SPEI depicts a worse
429 situation than WEPSI). The findings indicate that this behavior of WEPSI is observed among all
430 other sub-basins, as well.

431

432   **Figure 6.** SPI06, SPEI06, SRI06, and WEPSI06 time series based on the WEAP-derived
433 ET data for the Guajillo sub-basin (1980–2010).

434   The literature states that an SPI with 3- or 6-month steps can be considered as an
435 agricultural drought index (Khoshnazar et al., 2021; McKee et al., 1993; Vicente-Serrano, 2006).
436 It is also shown that SPI and SPEI, with 6-month time steps, have the highest correlation with each
437 other (Diaz et al., 2018). Additionally, we compared the river streamflow with WEPSI and SRI
438 for 3-, 6-, 9-, and 12-month time steps. We found that WEPSI06 and SRI06 were most related in
439 terms of low flow in the basin. Accordingly, we consider WEPSI06 representative of the
440 agricultural and hydrological drought conditions in the basin—WEPSI06 reflected a realistic
441 vision of the basin that links meteorological, agricultural, and hydrological drought.
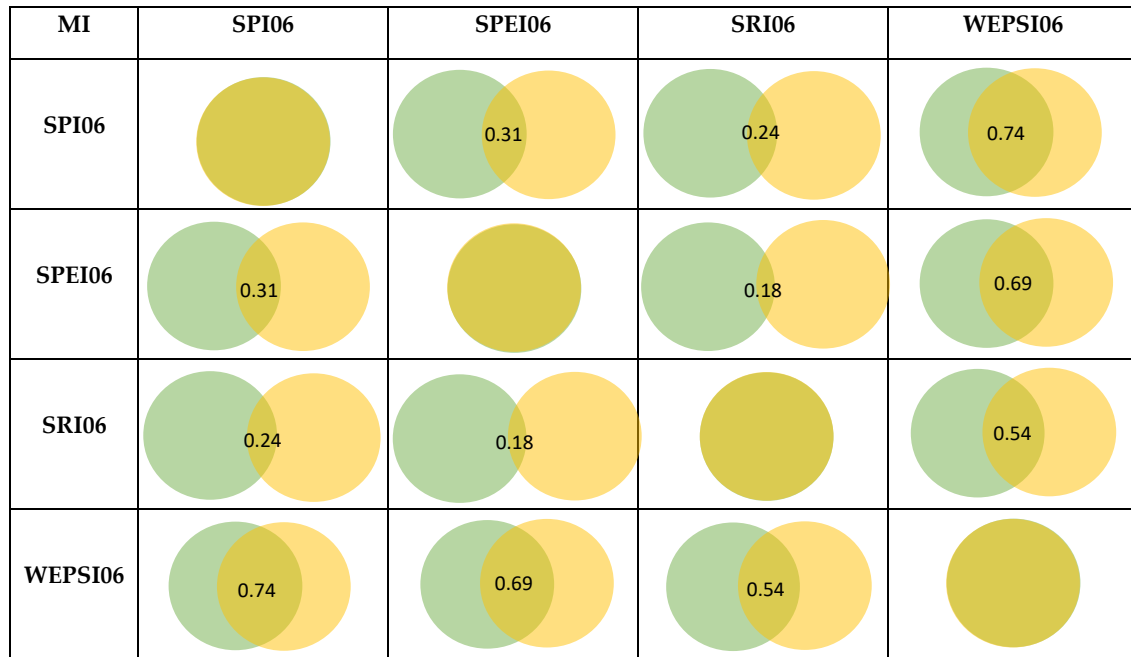
442   The correlation among the four drought indices is presented in Table 2. These correlations
443 are the averages of the eight sub-basins. The correlations between WEPSI06 and SPI06 (0.931),
444 WEPSI06 and SPEI06 (0.904), and WEPSI06 and SRI06 (0.783) are the highest. In comparison
445 with the other drought indices, WEPSI has the highest correlation with all drought indices, and the
446 correlation between SPEI06 and SRI06 (0.501) is the lowest.

447

Table 2. Correlation analysis

Drought indices	SPI06	SPEI06	SRI06	WEPSI06
SPI06	1	0.741	0.634	**0.931**
SPEI06	0.741	1	0.501	**0.904**
SRI06	0.634	0.501	1	**0.783**
WEPSI06	**0.931**	**0.904**	**0.783**	1

448   In addition to correlation analysis, MI was calculated among the drought indices (Section
449 2.6.2). As mentioned, MI was calculated to identify which drought index contains more
450 information about the others. MI is expressed in nat, the International System of Units unit for
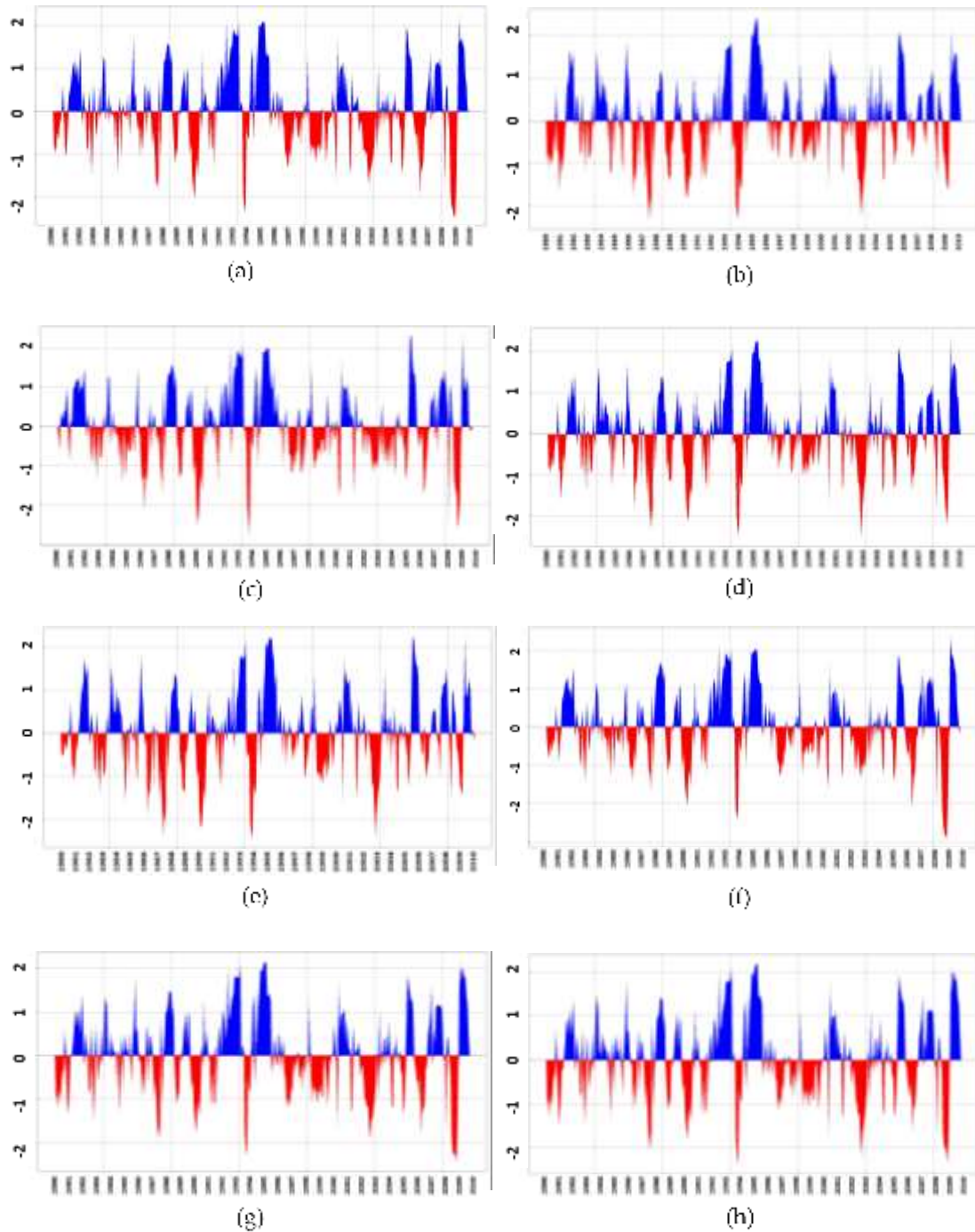451 entropy (details in Section 2.6.2).

452

453

454

455   Figure 7 depicts Venn diagrams that provide MI between drought indices. The values
456   presented in Figure 7 are the averages of the eight sub-basins. The highest MI is between WEPSI06
457   and SPI06, WEPSI06 and SPEI06, and WEPSI06 and SRI06, with 0.74, 0.69, and 0.54 nat,
458   respectively. The lowest MI is observed between SPEI06 and SRI06 (0.18 nat). The MIs between
459   SPI06 and SPEI06, and SPI06 and SRI06 are 0.31 and 0.24 nat, respectively. Accordingly,
460   WEPSI06 not only contains the highest amount of information about the two other meteorological
461   drought indices (SPI06 and SPEI06) but also covers the most information about the hydrological
462   conditions of the region (SRI06). SPEI06 and SPI06 send the lowest number of hydrological
463   signals in terms of drought. The results of the correlation analysis and MI suggest that WEPSI is
464   a drought index that identifies hydrological drought in the absence of R data.

MI	SPI06	SPEI06	SRI06	WEPSI06
SPI06		0.31	0.24	0.74
SPEI06	0.31		0.18	0.69
SRI06	0.24	0.18		0.54
WEPSI06	0.74	0.69	0.54	

465

466   **Figure 7.** Mutual information (MI) Venn diagram between SPI06, SPEI06, SRI06, and
467   WEPSI06. The intersection between two circles depicts the MI between two drought indices in
468   nat, the SI unit for entropy.

469   Figure 8a–h compares the time series of the WEAP-based WEPSI06 in the eight sub-basins
470   of the Lempa River basin for the period 1980–2010 (31 years). Based on Figure 8, the longest
471   drought (i.e., number of months in which the value of WEPSI is below the threshold of −1)
472   occurred in 2003, in general. The maximum drought frequency (3.54%) occurred in the Guajillo,
473   SS6, and Suquioyo sub-basins, with a total of 13 droughts over 31 years. The most severe drought
474   (i.e., aggregation of WEPSI values in sequent months at drought) occurred in Guajillo in December
475   1994.

Figure 8. Time series of WEPSI06 in the sub-basins: (a) Acelhuate, (b) Guajillo, (c) Lempa 1, (d) Lempa 2, (e) Lempa 3, (f) SS3, (g) SS6, and (h) Suquioyo.
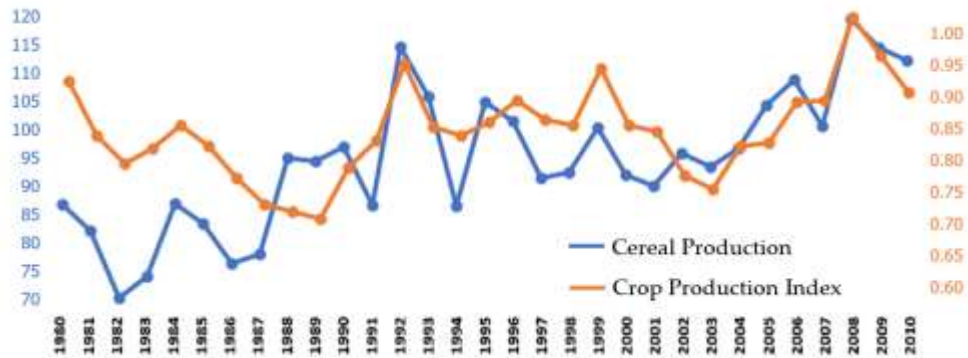
Figure 9 displays the variation of drought areas through the PDAs in the Lempa River basin for 31 years based on WEPSI06. The threshold of -1 was used to calculate drought in each WEPSI time series (i.e., a sub-basin is in drought if WEPSI06 ≤ -1; Table 1). Figure 9 shows some repetitive patterns in the behavior of droughts in the basin. Some years are in white cells, indicating the absence of PDA in those years, which are known as white years. By contrast, some other years show a tail (i.e., PDA occurs in some sequenced months, indicating long drought events).

Figure 9. Percentage of drought area (PDA) using WEPSI06 based on WEAP data in the Lempa River basin for the period 1980–2010.

As ENSO events are usually linked to major flood and drought episodes (Mera et al., 2018), we have applied this information to assess the performance of WEPSI. Drought events indicated by the PDA results (Figure 9) are compared with the EL Niño and La Niña years based on the Oceanic Niño Index (ONI) (National Oceanic and Atmospheric Administration (NOAA), 2021). ENSO events affect people and ecosystems across the globe via the production of secondary results that influence food supplies and prices, as well as forest fires, and create additional economic and political consequences (NOAA, 2021). Comparing the patterns of PDA based on WEPSI06 (Figure 9) and ONI shows that PDA shares similarities with La Niña in terms of white years, including weak La Niña in 1984, 2001, 2005, and 2006, moderate La Niña in 1995, 1996, 2000, and 2008, and strong La Niña in 1999. On the other hand, investigating the years with a drought tail reveals weak El Niño in 1980, 2004, 2007, 2009, and 2010, moderate El Niño in 1986, 1994, 2002, and 2003, strong El Niño in 1987, 1988, 1991, and 1992, and very strong El Niño in 1998. The consistency of the results provided by WEPSI06 with El Niño and La Niña years emphasize the good performance of WEPSI.

The fluctuation in cereal and crop production in El Salvador is shown in Figure 10 for the period 1980–2010 (31 years) (Worldbank, 2021).

Figure 10. Cereal production (million metric tons) and crop production index in El Salvador for the period 1980–2010 (31 years) (Khoshnazar et al., 2021).

As Figure 10 depicts, in 1984, 1988, 1990, 1992, 1995, 1999, 2002, 2006, and 2008, cereal production presented the local maximum amount compared with that in previous and subsequent years. On the other hand, the years 1982, 1986, 1989, 1991, 1994, 1997, 2001, 2003, and 2007 presented the local minimum. These years with the local minimum and maximum, aside from the years with descending and ascending cereal production amounts (compared with the previous year), were used for the comparison with drought indices' PDA. Our results endorse that the PDA of WEPSI06 based on WEAP model data detects six of the nine local maximums in El Salvador's cereal production evolution (when a year does not have at least two sequent months with a PDA value greater than 0% based on the drought index, and that year has a local maximum in the cereal production graph, the drought index is detecting the local maximum of cereal production), as well as six of the nine local minimums in cereal production fluctuation (when a year has some consecutive months with a PDA value greater than 0% based on the drought index, and that year has a local minimum in the cereal production graph, the drought index is detecting the local minimum of cereal production). This is while both SRI06 and SPEI06 detect four of the nine local maximums. SRI06 identifies five of the nine and SPEI06 reflects four of the nine local minimums of the graph. Finally, SPI06 does not detect a considerable number of critical points (i.e., the local maximum and minimum points) in El Salvador's cereal production graph. Besides, PDA based on WEPSI06 detects five years—1980, 1981, 1985, 2009, and 2010—when the tail of drought (at least two sequent months with a PDA greater than zero) is observed in them, and the amount of cereal production is lower than the previous year (i.e., the cereal production graph is descending); it also identifies that in 2005, which is a white year, the cereal production graph is ascending.

Generally, a growing pattern in cereal and crop production is observed during our study horizon. This is because cereal and crop productions do not depend on drought alone but are also influenced by other factors, such as agricultural land and technology. For example, El Salvador's agricultural land grew from 14,100 km^2 (or 68.05% of the land area) in 1980 to 15,350 km^2 (or 74.08% of the land area) in 2010 (Khoshnazar et al., 2021). There are some other descriptions for the rise or drop in the cereal production graph. For example, 1992 has a tail of drought in Figure 9, while it has a local maximum in Figure 10. That is because 1992 was the end of the civil war in El Salvador, which affected the agricultural activity and production of the country. Moreover, in 1997, which is a white year with a local minimum in Figure 10, a surge in coffee prices led to the replacement of other products with coffee and a drop in cereal production. By contrast, the poor harvests and falling prices (around 50%) of coffee in that year altered farming decisions, giving

539 rise to a local maximum in 1998 (in Figure 9), while the tail of drought was also observed in that
540 year in Figure 10 (Nationsencyclopedia, 2021).

541   As Figure 10 shows, the ascent and descent of the crop and cereal production graphs are
542 the same except in 1987 and 1988, when the crop graph is descending but the cereal graph is
543 ascending. There should be another probable occurrence or policy justifying this behavior of the
544 cereal production graph, while these years have a tail of drought in Figure 9. Furthermore, the
545 agricultural industry in El Salvador reported heavy losses because of rainfall and its consequences,
546 such as flood and supersaturation within our study horizon (Freshplaza, 2021). This can justify the
547 drop in cereal production in white years by PDA based on WEPSI06. For instance, in 1982,
548 hurricane Paul killed 1,625 people and caused \$520 million in damage in Central America,
549 including El Salvador. Similarly, hurricane Pauline in 1997 and tropical storm Arlene in 1993
550 impacted our studied basin (Carroll, 1998).

551   To sum up, PDA, based on WEPSI06, detects 85% of the cereal production drop and 70%
552 of the cereal production increase. Taking the discussed abnormal conditions into account, the PDA
553 based on WEPSI06 (Figure 9) is 81% consistent with the cereal production graph (Figure 10).

554   Regarding cereal production, the period between the first of April and the end of July is
555 the lean period in the El Salvador cereal calendar (Global Information and Early Warning System,
556 2021). Figure 9 demonstrates that tails of drought are observed in the lean period of cereal crops
557 in El Salvador—during 1981, 1994, 2003, and 2007, when a reduction in cereal production also
558 emerges. Additionally, the growing season, which starts from June and lasts until December
559 ("Global Information and Early Warning System,"), is also sensitive to WEPSI time-series
560 droughts, as shown by the decrease in cereal production. This sensitivity to drought, similar to
561 Daryanto et al.'s (Daryanto et al., 2017) statement, is observed in 10 years in Figure 10. On the
562 other hand, as the structure of WEPSI uses ET data, it implicitly determines soil moisture
563 variability and, therefore, vegetation water content, directly affecting agricultural droughts
564 (Vicente-Serrano et al., 2010). Indices that do not consider the role of temperature, and,
565 consequently heat, could not depict the impact of this critical environmental component on crop
566 survival, distribution, and productivity limits (Daryanto et al., 2017). This is while WEPSI
567 implicitly takes the role of temperature into account and thus could be used for agricultural targets.

568   These observations indicate that the results of WEPSI06 could be used for the assessment
569 of agricultural drought.

570   3.2 Significance of this study

571   Because of its inputs, WEPSI can indirectly take the climate change effect into account.
572 WEPSI softens the performance of the SPEI because it uses ET_w instead of evaporative demand
573 (i.e., ET_p). Accordingly, WEPSI can detect some events that are not captured by the SPI but can
574 eliminate some others indicated by the SPEI that are derived by excessive values of ET_p.

575   Meteorological drought indices, such as the SPI and SPEI, describe climatic anomalies
576 without considering their hydrologic context (Kim and Rhee, 2016). Hydrological drought indices,
577 such as the SRI, represent the impact of climate anomalies on present hydrologic conditions, as
578 they are controlled by physical processes on the surface (Shukla and Wood, 2008). Our results
579 show a high correlation and MI between WEPSI06 and SRI06. These results indicate that WEPSI
580 can depict a more accurate land surface status by linking meteorological and hydrological drought
581 indices.

582 ET affects R (Vicente-Serrano et al., 2010), so the SRI can depict ET_a indirectly. Then,
583 WEPSI, which, on the one hand, relatively reflects the SRI status and, on the other hand, uses ET,
584 can indicate moisture conditions on the land surface. Additionally, our results showed a high
585 similarity between the SRI with the 6-month time step (SRI06) and the Lempa River streamflow,
586 suggesting that SRI06 reflects the basin's most accurate condition. The results again indicate that
587 WEPSI can be used for agricultural drought assessments.

588 The proposed WEPSI drought index meets all requirements suggested by Nkemdirim and
589 Weber for a drought index (Nkemdirim and Weber, 1999; Vicente-Serrano et al., 2010), including
590 its use for different purposes. Drought characteristics, such as drought severity, intensity, and
591 duration (the start and the end of the phenomenon), can also be calculated with WEPSI.
592 Furthermore, WEPSI can be calculated worldwide and under various climates and can provide a
593 spatial and temporal depiction of drought variation.

4 Conclusions

595 This research introduced WEPSI, which uses WS as its input. WS is calculated using P and
596 ET_w. We embed ET_w into the structure of WEPSI to account for the water demand and P for the
597 water supply. This paper also presents a procedure for ET_w calculation based on the asymmetric
598 CR that links ET_p, ET_a, and ET_w.

599 We tested WEPSI in the Lempa River basin, which is the longest river in Central America.
600 The basin is sub-divided into eight sub-basins for its modeling with the WEAP system. ET_w is
601 calculated with ET_p and ET_a derived from WEAP.

602 We compared WEPSI with two meteorological drought indices (SPI and SPEI) and a
603 hydrological drought index (SRI) via data derived from WEAP. The performance evaluation
604 procedure includes a correlation coefficient (r) and an approach based on MI. The results show
605 that WEPSI has the highest r and MI compared with the three other indices, indicating that WEPSI
606 can be used for meteorological, agricultural, and hydrological drought monitoring.

607 Finally, drought events based on WEPSI were compared with El Niño–La Niña years, as
608 well as with El Salvador's annual cereal production. The results indicate that WEPSI is also helpful
609 for agricultural drought assessments because it captures the most critical points of El Salvador's
610 cereal production (i.e., the local maximum and minimum points).

611 These research outcomes are useful for researchers and policymakers in drought
612 calculation, monitoring, risk assessment, and forecasting. As a future research direction, the
613 application of remote sensing data in calculating WEPSI can be investigated to facilitate the
614 application of WEPSI in other basins. We also suggest testing WEPSI in other case studies and
615 with other purposes. WEPSI's application for drought risk assessment is likewise foreseen.

5 Acknowledgments

620 **6 Author contributions**

621 AK: conceptualization, methodology, investigation, data processing, validation, software,
622 writing—original draft; GACP: conceptualization, project administration, supervision and review;
623 VD: conceptualization, methodology, data processing, writing—review and editing; MA:
624 conceptualization, methodology and review. All authors have read and agreed to the published
625 version of the manuscript.

626 **References**

627

628 Al Balasmeh, O., Babbar, R., and Karmaker, T. (2020). A hybrid drought index for drought
629 assessment in Wadi Shueib catchment area in Jordan. *Journal of Hydroinformatics, 22*(4),
630 937-956.
631 Aminzadeh, M., and Or, D. (2014). Energy partitioning dynamics of drying terrestrial surfaces.
632 *Journal of Hydrology, 519*, 1257-1270.
633 Aminzadeh, M., Roderick, M. L., and Or, D. (2016). A generalized complementary relationship
634 between actual and potential evaporation defined by a reference surface temperature. *Water
635 Resources Research, 52*(1), 385-406.
636 Bouchet, R. J. (1963). Evapotranspiration réelle et potentielle, signification climatique. *IAHS Publ,
637 62*, 134-142.
638 Brito, S. S. B., Cunha, A. P. M., Cunningham, C., Alvalá, R. C., Marengo, J. A., and Carvalho, M.
639 A. (2018). Frequency, duration and severity of drought in the Semiarid Northeast Brazil
640 region. *International Journal of Climatology, 38*(2), 517-529.
641 Carroll, A. (1998). Natural hazards of North America. Retrieved from
642 https://catalogue.nla.gov.au/Record/7045960
643 Corzo Perez, G., Diaz, V., and Laverde, M. (2018). Spatiotemporal hydrological analysis. *Int J
644 Hydro, 2*(1), 25-26.
645 Corzo Perez, G., Van Huijgevoort, M., Voß, F., and Van Lanen, H. (2011). On the spatio-temporal
646 analysis of hydrological droughts from global hydrological models. *Hydrology and Earth
647 System Sciences, 15*(9), 2963-2978.
648 Daryanto, S., Wang, L., and Jacinthe, P.-A. (2017). Global synthesis of drought effects on cereal,
649 legume, tuber and root crops production: A review. *Agricultural Water Management, 179*,
650 18-33.
651 Dash, S. S., Sahoo, B., and Raghuwanshi, N. S. (2021). How reliable are the evapotranspiration
652 estimates by Soil and Water Assessment Tool (SWAT) and Variable Infiltration Capacity
653 (VIC) models for catchment-scale drought assessment and irrigation planning? *Journal of
654 Hydrology, 592*, 125838.
655 Dhungel, S., and Barber, M. E. (2018). Estimating calibration variability in evapotranspiration
656 derived from a satellite-based energy balance model. *Remote Sensing, 10*(11), 1695.
657 Diaz, V., Corzo Perez, G., Van Lanen, H. A., and Solomatine, D. (2018). *Comparative analysis of
658 two evaporation-based drought indicators for large-scale drought monitoring.* Paper
659 presented at the EGU General Assembly Conference Abstracts.
660 Diaz, V., Corzo Perez, G., Van Lanen, H. A., Solomatine, D., and Varouchakis, E. A. (2020). An
661 approach to characterise spatio-temporal drought dynamics. *Advances in Water Resources,
662 137*, 103512.
663 El Salvador's Ministry of Environment and Natural Resources (MARN). (2019). Water
664 Resources Maps. Retrieved from

https://web.archive.org/web/20090422151648/http://snet.gob.sv/cd2/SeccionSIG/map_hi.htm

El Salvador's Ministry of Environment and Natural Resources (MARN). (2020). Retrieved from https://www.marn.gob.sv/

Fisher, J. B., Whittaker, R. J., and Malhi, Y. (2011). ET come home: potential evapotranspiration in geographical ecology. *Global Ecology and Biogeography, 20*(1), 1-18.

Fostering Water Security in the Trifinio Region: Promoting the formulation of a TDA/SAP for its transboundary Lempa River Basin. (2019). Retrieved from https://www.thegef.org/project/fostering-water-security-trifinio-region-promoting-formulation-tdasap-its-transboundary

Freshplaza (2021). Agricultural industry in El Salvador reports heavy losses due to rainfall. Retrieved from https://www.freshplaza.com/article/9267702/agricultural-industry-in-el-salvador-reports-heavy-losses-due-to-rainfall/

Global Information and Early Warning System (2021). Retrieved from http://www.fao.org/giews/countrybrief/country.jsp?code=SLV&lang=en

Granger, R. (1989). A complementary relationship approach for evaporation from nonsaturated surfaces. *Journal of Hydrology, 111*(1-4), 31-38.

Han, S., and Tian, F. (2020). A review of the complementary principle of evaporation: from the original linear relationship to generalized nonlinear functions. *Hydrology and Earth System Sciences, 24*(5), 2269-2285.

Helman, P., and Tomlinson, R. (2018). Two centuries of climate change and climate variability, East Coast Australia. *Journal of Marine Science Engineering, 6*(1), 3.

Hernández, W. (2005). Nacimiento y Desarrollo del río Lempa. *MARN/SNET*.

Homdee, T., Pongput, K., and Kanae, S. (2016). A comparative performance analysis of three standardized climatic drought indices in the Chi River basin, Thailand. *Agriculture and Natural Resources, 50*(3), 211-219.

Jennewein, J. S., and Jones, K. W. (2016). Examining 'willingness to participate' in community-based water resource management in a transboundary conservation area in Central America. *Water Policy, 18*(6), 1334-1352.

Kahler, D. M., and Brutsaert, W. (2006). Complementary relationship between daily evaporation in the environment and pan evaporation. *Water Resources Research, 42*(5).

Karim, M. R., and Rahman, M. A. (2015). Drought risk management for increased cereal production in Asian least developed countries. *Weather and Climate Extremes, 7*, 24-35.

Khoshnazar, A., Corzo Perez, G. A., and Diaz, V. (2021). Spatiotemporal Drought Risk Assessment Considering Resilience and Heterogeneous Vulnerability Factors: Lempa Transboundary River Basin in The Central American Dry Corridor. *Journal of Marine Science and Engineering, 9*(4), 386.

Kim, D., and Rhee, J. (2016). A drought index based on actual evapotranspiration from the Bouchet hypothesis. *Geophysical Research Letters, 43*(19), 10,277-210,285.

Kim, J.-S., Jain, S., Lee, J.-H., Chen, H., and Park, S.-Y. (2019). Quantitative vulnerability assessment of water quality to extreme drought in a changing climate. *Ecological Indicators, 103*, 688-697.

Koppa, A., Alam, S., Miralles, D. G., and Gebremichael, M. (2021). Budyko-Based Long-Term Water and Energy Balance Closure in Global Watersheds From Earth Observations. *Water Resources Research, 57*(5), e2020WR028658.

710 Kumar, P., Masago, Y., Mishra, B. K., and Fukushi, K. (2018). Evaluating future stress due to
711   combined effect of climate change and rapid urbanization for Pasig-Marikina River,
712   Manila. *Groundwater for Sustainable Development, 6*, 227-234.
713 Lewis, J., Rowland, J., and Nadeau, A. (1998). Estimating maize production in Kenya using NDVI:
714   some statistical considerations. *International Journal of Remote Sensing, 19*(13), 2609-
715   2617.
716 Lu, Z., Zhao, Y., Wei, Y., Feng, Q., and Xie, J. (2019). Differences among evapotranspiration
717   products affect water resources and ecosystem management in an Australian catchment.
718   *Remote Sensing, 11*(8), 958.
719 McKee, T. B., Doesken, N. J., and Kleist, J. (1993). *The relationship of drought frequency and*
720   *duration to time scales.* Paper presented at the Proceedings of the 8th Conference on
721   Applied Climatology.
722 Mera, Y. E. Z., Vera, J. F. R., and Pérez-Martín, M. Á. (2018). Linking El Niño Southern
723   Oscillation for early drought detection in tropical climates: The Ecuadorian coast. *Science*
724   *of The Total Environment, 643*, 193-207.
725 Mukherjee, S., Mishra, A., and Trenberth, K. E. (2018). Climate change and drought: a perspective
726   on drought indices. *Current Climate Change Reports, 4*(2), 145-163.
727 National Oceanic and Atmospheric Administration (NOAA) (2021). Retrieved from
728   https://www.noaa.gov/education/resource-collections/weather-atmosphere/el-nino
729 Nationsencyclopedia (2021). El Salvador - Agriculture Retrieved from
730   https://www.nationsencyclopedia.com/economies/Americas/El-Salvador-
731   AGRICULTURE.html
732 Nkemdirim, L., and Weber, L. (1999). Comparison between the droughts of the 1930s and the
733   1980s in the southern prairies of Canada. *Journal of Climate, 12*(8), 2434-2450.
734 Oti, J. O., Kabo-Bah, A. T., and Ofosu, E. (2020). Hydrologic response to climate change in the
735   Densu River Basin in Ghana. *Heliyon, 6*(8), e04722.
736 Palmer, W. C. (1965). *Meteorological drought* (Vol. 30): US Department of Commerce, Weather
737   Bureau.
738 Palmer, W. C. (1968). Keeping track of crop moisture conditions, nationwide: the new crop
739   moisture index.
740 Priestley, C. H. B., and Taylor, R. J. (1972). On the assessment of surface heat flux and evaporation
741   using large-scale parameters. *Monthly weather review, 100*(2), 81-92.
742 Seiber, J., and Purkey, D. (2015). WEAP—Water Evaluation and Planning System User Guide for
743   WEAP 2015. *Stockholm Environment Institute*.
744 Shukla, S., and Wood, A. W. (2008). Use of a standardized runoff index for characterizing
745   hydrologic drought. *Geophysical Research Letters, 35*(2).
746 Sorí, R., Vázquez, M., Stojanovic, M., Nieto, R., Liberato, M. L., Gimeno, L. J. N. H., and
747   Sciences, E. S. (2020). Hydrometeorological droughts in the Miño–Limia–Sil
748   hydrographic demarcation (northwestern Iberian Peninsula): the role of atmospheric
749   drivers. *20*(6), 1805-1832.
750 Speich, M. J. (2019). Quantifying and modeling water availability in temperate forests: a review
751   of drought and aridity indices. *iForest-Biogeosciences and Forestry, 12*(1), 1.
752 Vergara, J. R., and Estévez, P. A. (2014). A review of feature selection methods based on mutual
753   information. *Neural computing and applications, 24*(1), 175-186.
754 Vicente-Serrano, S. M. (2006). Differences in spatial patterns of drought on different time scales:
755   an analysis of the Iberian Peninsula. *Water resources management, 20*(1), 37-60.

756   Vicente-Serrano, S. M., Beguería, S., and López-Moreno, J. I. (2010). A multiscalar drought index
757   sensitive to global warming: the standardized precipitation evapotranspiration index.
758   *Journal of Climate, 23*(7), 1696-1718.
759   Vicente-Serrano, S. M., Miralles, D. G., Domínguez-Castro, F., Azorin-Molina, C., El Kenawy,
760   A., McVicar, T. R., Peña-Gallardo, M. (2018). Global assessment of the Standardized
761   Evapotranspiration Deficit Index (SEDI) for drought analysis and monitoring. *Journal of
762   Climate, 31*(14), 5371-5393.
763   Wang, D., Hejazi, M., Cai, X., and Valocchi, A. J. (2011). Climate change impact on
764   meteorological, agricultural, and hydrological drought in central Illinois. *Water Resources
765   Research, 47*(9).
766   Wang, Y., Yang, J., Chen, Y., Su, Z., Li, B., Guo, H., and De Maeyer, P. (2020). Monitoring and
767   Predicting Drought Based on Multiple Indicators in an Arid Area, China. *Remote Sensing,
768   12*(14), 2298.
769   Wells, N., Goddard, S., and Hayes, M. J. (2004). A self-calibrating Palmer drought severity index.
770   *Journal of Climate, 17*(12), 2335-2351.
771   Wen, W., Timmermans, J., Chen, Q., and van Bodegom, P. M. (2021). A Review of Remote
772   Sensing Challenges for Food Security with Respect to Salinity and Drought Threats.
773   *Remote Sensing, 13*(1), 6.
774   Wilhite, D. A., and Glantz, M. H. (1985). Understanding: the drought phenomenon: the role of
775   definitions. *Water international, 10*(3), 111-120.
776   Worldbank (2021). Cereal production (metric tons) - El Salvador. Retrieved from
777   https://data.worldbank.org/indicator/AG.PRD.CREL.MT?locations=SV
778   Xiao, M., Yu, Z., Kong, D., Gu, X., Mammarella, I., Montagnani, L., Lohila, A. (2020). Stomatal
779   response to decreased relative humidity constrains the acceleration of terrestrial
780   evapotranspiration. *Environmental Research Letters, 15*(9), 094066.
781   Yihdego, Y., Vaheddoost, B., and Al-Weshah, R. A. (2019). Drought indices and indicators
782   revisited. *Arabian Journal of Geosciences, 12*(3), 69.
783   Zargar, A., Sadiq, R., Naser, B., and Khan, F. I. (2011). A review of drought indices.
784   *Environmental Reviews, 19*(NA), 333-349.
785   Zhang, J., Bai, Y., Yan, H., Guo, H., Yang, S., and Wang, J. (2020). Linking observation,
786   modelling and satellite-based estimation of global land evapotranspiration. *Big Earth Data,
787   4*(2), 94-127.
788   Zheng, C., Jia, L., Hu, G., and Lu, J. (2019). Earth Observations-Based Evapotranspiration in
789   Northeastern Thailand. *Remote Sensing, 11*(2), 138.

790